Analysis of the Pressure-Pulse Propagation in Rock: a New Approach to Simultaneously Determine Permeability, Porosity, and Adsorption Capacity

Chaolin Wang[1] · Lehua Pan[2] · Yu Zhao[1] · Yongfa Zhang[3] · Weike Shen[3]

[1] College of Civil Engineering, Guizhou University, Guiyang 550025, Guizhou, China [2] Earth and Environmental Sciences Area, Lawrence Berkeley National Laboratory, Berkeley, CA 94720, USA [3] School of Civil Engineering, Chongqing University, Chongqing 400044, China

Abstract

Permeability estimation from pressure-pulse decay method is complicated by two facts: (1) the decay curve often deviates from the single-exponential behavior in the early time period and (2) possible existence of gas adsorption. Both the two factors cause significant permeability error in most of pressure-pulse decay methods. In this paper, we first present a thorough analysis of pressure-pulse propagation process to reveal the mechanism behind the early time and later time behaviors of pressure decay curve. Inspired by the findings from these analyses, a new scaled pressure is proposed which can: (1) be easily used to distinguish the early time and later time data and (2) make the decay curves of all cases into a single 1:1 straight line for later time. A new data-proceeding method, which calculates the apparent porosity and permeability using the same set of measured data, is then developed. The new method could not only remove the effects of the adsorption on the permeability estimation, but also identify the apparent porosity as well as proper adsorption model and parameters. The proposed method is verified by comparing with true values and calculated values through numerical simulations that cover variations in typical rock properties (porosity, permeability, slippage, and adsorption) and the experiment configurations. It is found that the new method is accurate and reliable for all test cases, whereas the Brace's and Cui's approaches may cause permeability error in some cases. Finally, the new method has been successfully applied to real data measured in pressure-pulse decay experiments involving different types of rocks and gases.

List of Symbols

a

The ratio of apparent pore volume to upstream volume

A

Sample cross-sectional area

b

The ratio of apparent pore volume to downstream volume

c

Gas compressibility

k

True permeability

k_a

Apparent permeability

L

Sample length

m_L

The maximum gas adsorption capacity

M

The total gas mass in the control volume

p

Gas pressure in the sample

p_c

Confining pressure

p_f

Final equilibrium pressure

p_L

Langmuir pressure

p_m

Mean gas pressure

p_1

The pressure of upstream chamber

p_2

The pressure of downstream chamber

Δp

Initial pressure difference

Δp_D

Dimensionless pressure difference

$p*$

New scaled pressure decay

S_m

The mth term of Eq. ([12](#))

t

Real time

t_D

Dimensionless time

$t*$

New scaled time

V_s

The volume of sample pore

V_u

The volume of upstream chamber

V_d

The volume of downstream chamber

x

The distance along the sample from the upstream end

z

Gas compressibility factor

μ

Gas viscosity

λ

Klinkenberg coefficient

ρ_g

Gas density

ρ_R

Rock density

ψ

The mass of gas adsorbed per unit mass of rock

ϕ

True porosity

ϕ_a

Apparent porosity

ϕ_{ad}

The equivalent porosity due to gas adsorption

θ_m

The roots of Eq. (13)

η

The contribution of first term in Eq. (12) to all term

1 Introduction

Permeability estimation of reservoir rocks is critical for applications in unconventional oil and gas recovery (Karacan 2008; Jin et al. 2017; Fei et al. 2018), geological storage facilities for CO_2 (Pan et al. 2017; Kim et al. 2017, 2018), and seals for nuclear waste repositories (Berlepsch and Haverkamp 2016; Nasir et al. 2017; Zheng et al. 2017). Currently, the steady-flow method and the transient-flow method are two major techniques for permeability measurement (Sander et al. 2017). The steady-flow method consists of imposing a constant pressure gradient to a sample and measures the flow rates. However, the steady-flow technology is not adequate for tight rocks with low permeability, such as shale and higher rank coals, because the flow rates across the tight rock samples are often too small to be measured, and the tests are fairly time-consuming and inaccurate. Therefore, the transient-flow method based on the pressure-pulse decay signal, which is easier to measure, becomes the preferred option.

The pressure-pulse decay technique was initially proposed by Brace et al. (1968) for the determination of permeability in tight rocks. This technique is based on the analysis of the differential pressure between the upstream and downstream (Fig. 1). In a pulse decay test, the whole test system is kept at a uniform pore pressure for a period to get an equilibrium condition at first. Then, the pressure of upstream (or downstream) is increased (or decreased) to a specified level to create an initial pressure difference. The pressure responses at both ends are recorded after the valve is opened. The test ends when the upstream–downstream pressure difference becomes very small.

The permeability can then be estimated from the pressure-pulse decay curve (the upstream–downstream pressure difference with time) using mathematical solutions of the related flow problem. The standard exponential decay solution (often called as the Brace's solution) was first developed by Brace et al. (1968) by assuming that the pressure gradient is constant along the length of the sample, although it is a function of time and that the pore volume of the sample can be neglected. Hsieh et al. (1981) obtained a general solution of the 1-D flow problem without the simplifications used by Brace. Dicker and Smits (1988) expressed the general solution in terms of dimensionless time and pressure difference for easier analysis. Jones (1997) introduced a factor "f" to make Dicker and Smits later time solution in a similar form of Brace's solution. Recently, some optimized pressure decay methods were developed. Metwally and Sondergeld (2011) implemented a new technique to simultaneously measure the permeability and storage parameters of tight rock samples by creating an infinite storage capacity for the upstream chamber. Yang et al. (2015) suggested that only one chamber should be used in pulse pressure tests to simplify the experiment configurations. Hannon (2016) provided a bi-directional model of pressure-pulse-decay permeametry, which reaches equilibrium much faster than the standard pressure-pulse decay.
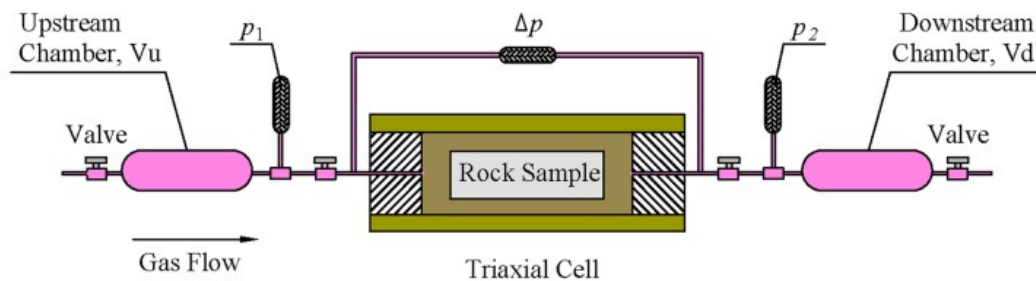

Fig. 1 Schematic sketch of the pressure-pulse decay technique. The sample is first in equilibrium and then opens the valve between the upstream chamber and the sample to let fluid flowing from the upstream chamber to the downstream chamber through the sample driven by Δp

The estimation of permeability from the measured pressure-pulse decay data is complicated by the fact that the decay curve will often deviate from the single-exponential behavior in the early time period (Fig. 2). Considerable error may result if early time data are included for permeability calculation (Feng 2017), because most of methods discussed above (Chen and Stagg 1984; Jones 1997; Yang et al. 2015; Feng 2017) require that only the late-time measurements are used for permeability calculation and the early time data, although the early time measurements may contain important information about the rock samples (Kamath et al. 1992; He and Ling 2016; Zhao et al. 2017), should be discarded. However, the timepoint differentiating the early time and late-time behavior has not been clearly defined and was often somewhat arbitrary in the literature. Although Hsieh et al. (1981) found that for cases with the ratio of the compressive storage within the sample to the compressive storage in the upstream reservoir less

than 10, the early time solution is applicable for the dimensionless time [defined in Eq. (14)] less than 0.2, while the later time solution is applicable for the dimensionless time larger than 0.2, this criterion cannot be used in practice, because the dimensionless time itself contains the permeability which is unknown when we need to decide the subset of later time data.
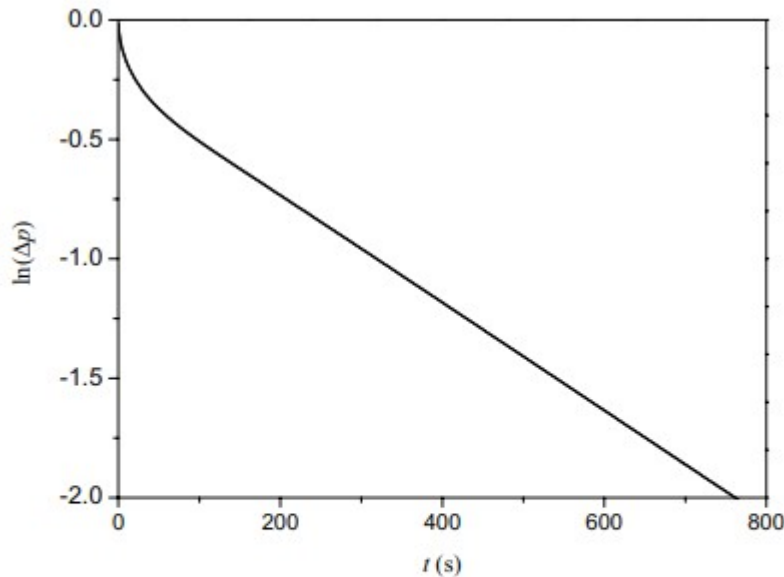

Fig. 2 Typical pressure-pulse decay curve during pressure-pulse decay experiment (data come from Test 2 at confining pressure of 5 MPa in Sect. 5). The later time upstream–downstream pressure difference shows exponential decay with time (i.e., straight line in semi-log plotting)

The estimation of permeability from the measured pressure-pulse decay data is further complicated due to possible existence of gas adsorption, a unique feature of kerogen-bearing rocks. In those rocks, free gas will lose, because kerogen has a very high internal surface area for gas adsorption. In other words, the adsorption provides additional gas storage of the sample. Therefore, the estimated permeability from the pressure-pulse decay method may be incorrect if adsorption effects are not considered for those rocks with adsorbable gas. Cui et al. (2009) proposed an approach by incorporating the Langmuir model into the Dicker and Smits solution to consider adsorption effects. It becomes apparent that additional effort is required due to the increased number of input Langmuir parameters. Feng et al. (2017) tried to eliminate the effect of compressibility storage and sorption on permeability measurement by introducing a bi-directional pressure-pulse test (i.e., to create same magnitude but opposite direction of pressure pulses in each chamber concurrently). However, although the bi-directional pulse method could eliminate the net changes in compressive storage and sorption by equaling the initial pressure and the final pressure, the effects of spatially distributed adsorption/desorption on the upstream and the downstream

pressure before ending of the pressure decay may not be properly cancelled each other, so that the method was found not to be effective in removing the effects of sorption on the permeability measurement.

In this paper, we presented a thorough analysis of the pressure-pulse propagation process to reveal the mechanism behind the early time and later time behaviors of pressure decay curve and the reasons why the pressure decay curves are controlled by the governing equation using the apparent permeability and the apparent porosity if adsorption and gas slippage are existing. Inspired by the findings from these analyses, we proposed a new scaling method that can make the decay curves of all cases into a single 1:1 straight line for later time, which facilitate a new approach for inferring permeability and other related parameters from the measured pressure decay curve. The new approach can automatically select the later time data from the raw measurements and calculate the permeability and its standard deviation as well as apparent porosity and adsorption capacity. The new approach could not only remove the effects of the adsorption on the determination of the permeability, but also identify proper adsorption model and parameters with multiple pressure-pulse tests. We then performed a series of numerical simulations of pressure decay experiments with various rock properties under typical experiment settings to evaluate the accuracy and the robustness of the proposed approach. Finally, the new approach (and the associated code, documented in "Appendix") is successfully applied to processing the real data obtained from several pressure decay experiments involving two types of rocks and two types of gases under different confining pressure and pore pressure.

2 The Principles of Pressure-Pulse Decay Method: Apparent Porosity and Permeability

The pressure-pulse decay method involves a closed system that consists of two chambers, under different initial pressures, which are connected through the rock core (Fig. 1). The initial pressure pulse will propagate through the rock core from the upstream chamber to the downstream chamber. The fundamental process can be seen as one-dimensional gas flow through the porous core sample, which can be described by the following governing equation:

$$\frac{\partial M}{\partial t} = \frac{\partial}{\partial x} \cdot \left(\frac{k_a \rho_g}{\mu} \frac{\partial p}{\partial x} \right), \tag{1}$$

where M is the total gas mass in the control volume, kg/m^3; ρ_g is the density of gas, kg/m^3; t is time, s; μ is gas viscosity, Pa s; p is the gas pressure, Pa; and k_a is apparent permeability, m^2, which can be expressed as a general form including gas-slippage effects (Klinkenberg 1941):

$$k_a = k \left(1 + \frac{\lambda}{p_m} \right), \tag{2}$$

where k is true permeability, m²; λ is Klinkenberg coefficient, Pa; and p_m is a constant pressure, representing the mean gas pressure, Pa.

The gas mass in the control volume (M) consists of free-phase gas in pore space ($\phi\rho_g$) and adsorbed gas by rock matrix [the second term on the right of Eq. (3)], which can be described as follows:

$$M = \phi\rho_g + (1 - \phi)\,\rho_R\psi\,(p)\,,$$

(3)

where ρ_R is the density of rock sample, kg/m³; $\psi(p)$ is the mass of gas adsorbed per unit mass of rock, kg of gas/kg of matrix material; and $(1 - \phi)\rho_R$ represents the mass of rock matrix in the control volume.

Substituting Eq. (3) into Eq. (1) and assuming that spatial changes in ρ_g, k_a, and μ are negligible yields

$$\left[\phi\frac{d\rho_g}{dp} + (\rho_g - \rho_R\psi\,(p))\frac{d\phi}{dp} + (1 - \phi)\,\rho_R\psi'\,(p)\right]\frac{\partial p}{\partial t} = k_a\frac{\rho_g}{\mu}\frac{\partial^2 p}{\partial x^2}.$$

(4)

Considering that the changes in true porosity due to a small pressure pulse in test can be negligible (i.e., $\frac{d\phi}{dp}$ =0), the second term on the left side of Eq. (4) can be reasonably omitted. As a result, the governing equation (4) can be expressed as by introducing the concept of apparent porosity:

$$\phi_a\frac{\partial p}{\partial t} = \frac{k_a}{c\mu}\frac{\partial^2 p}{\partial x^2},$$

(5)

where the apparent porosity is a summation of true porosity, ϕ, and the equivalent porosity due to gas adsorption, ϕ_{ad}:

$$\phi_a = \phi + \phi_{ad}.$$

(6)

In addition, the equivalent porosity due to gas adsorption is a measure of the gas adsorption capacity of a sample in terms of "porosity" in Eq. (5). It can be defined as a function of the gradient of gas adsorption with respect to gas pressure:

$$\phi_{ad} = \frac{\rho_R\,(1 - \phi)}{c\rho_g}\psi'\,(p)\,,$$

(7)

where c is the gas compressibility $\left(c = \frac{1}{\rho_g}\frac{d\rho_g}{dp}\right)$.

Note that the equivalent porosity due to adsorption is a virtual porosity to account for the adsorption in the mass balance equation (7) that controls the gas transport in the rock sample. It is a mathematic equivalent variable representing the adsorption capacity in terms of porosity and there is no

physical volume or density of adsorbed gas is involved in this concept. The equivalent porosity due to adsorption could be as large as many times of the true porosity, not necessary limited by the maximum (true) porosity of 1. Cui et al. (2009) provided a number of examples of larger equivalent porosity, although they called it as effective adsorption porosity. Unlike Cui et al. (2009) who derived an equation to calculate the equivalent porosity based on Langmuir adsorption model, Eq. (7), here is a general relationship between the equivalent porosity and the adsorption. The concept of the equivalent porosity can be applied to all cases including Langmuir adsorption or even the case there is no closed form adsorption model exists. Gas ad-/desorption has been studied extensively and several analytic/semi-analytic models have been developed for predicting gas sorption behavior (Duong 1998), such as Langmuir sorption, Freundlich sorption, BET (Brunauer, Emmett, and Teller) sorption, and Dubinin–Astakhov (D–A) sorption. If the adsorption can be described by the Langmuir model, the mass of gas adsorbed ψ can be calculated as a function of pressure (Zhang et al. 2008; Moridis and Pruess 2014; Ma et al. 2017):

$$\psi(p) = \frac{m_L p}{p + p_L}, \tag{8a}$$

where m_L describes the maximum gas adsorption capacity, kg of gas/kg of matrix material; p_L is the pressure at which half of this capacity is reached, Pa; p is the pressure in the sample, Pa. In this case, the equivalent porosity can be calculated as

$$\phi_{ad} = \frac{\rho_R (1 - \phi)}{c \rho_g} \frac{m_L p_L}{(p + p_L)^2}. \tag{8b}$$

The equations for calculating the equivalent porosity due to adsorption for other adsorption models are listed in Table 1.

Table 1 Equations for calculating the equivalent porosity due to adsorption for adsorption models

Sorption model	Function	Equivalent porosity due to adsorption
Langmuir model	$\psi(p) = \frac{m_L p}{p_L + p}$	$\phi_{ad} = \frac{\rho_R(1-\phi)}{c\rho_g} \frac{m_L p_L}{(p+p_L)^2}$
Freundlich model	$\psi(p) = K p^n$	$\phi_{ad} = \frac{\rho_R(1-\phi)}{c\rho_g} K p^{n-1}$
BET model	$\frac{1}{\psi(p)(p_0/p-1)} = \frac{1}{V_m C} + \frac{C-1}{V_m C}\frac{p}{p_0}$	$\phi_{ad} = \frac{\rho_R(1-\phi)}{c\rho_g}\left\{ \frac{C p_0 V_m p}{(p-p_0)^2 (p_0 - p + Cp)} - \frac{C p_0 V_m}{(p-p_0)(p_0 - p + Cp)} + \frac{C p_0 V_m p (C-1)}{(p-p_0)(p_0 - p + Cp)^2} \right\}$
D–A model	$\psi(p) = V_0 \exp\left[-D\left\{\ln\left(\frac{p_0}{p}\right)^2\right\}\right]$	$\phi_{ad} = \frac{\rho_R(1-\phi)}{c\rho_g}\frac{2DV_0}{p}\exp\left[-D\left\{\ln\left(\frac{p_0}{p}\right)^2\right\}\right]$

Finally, the one-dimensional gas flow process in the pressure-pulse decay method can be described by the governing equation (5) completed by the following initial and boundary conditions:

$$p(x,0) = p_2(0) \quad \text{for } 0 < x < L, \tag{9a}$$

$$p(0,t) = p_1(t) \quad \text{for } t \geq 0, \tag{9b}$$

$$p(L,t) = p_2(t) \quad \text{for } t \geq 0, \tag{9c}$$

$$\frac{dp_1}{dt} = \frac{k_a}{c\mu\phi_a L} \frac{V_S}{V_u} \left.\frac{\partial p}{\partial x}\right|_{x=0}, \quad \text{for } t > 0, \tag{9d}$$

$$\frac{dp_2}{dt} = -\frac{k_a}{c\mu\phi_a L} \frac{V_S}{V_d} \left.\frac{\partial p}{\partial x}\right|_{x=L}, \quad \text{for } t > 0, \tag{9e}$$

where x denotes the distance along the sample from the upstream end, m; L refers sample length, m; V_s, V_u, and V_d refer the volume of sample pore, upstream chamber and downstream chamber, m³, respectively; p_1 and p_2 are the pressure of upstream chamber and downstream chamber, Pa.

Note that Eqs. (5) and (9a–9e) have the same mathematical forms of the governing equations first presented by Brace et al. (1968). Therefore, the Brace's simple solution, as well as Hsieh's general solutions, can be readily presented as solutions of Eq. (5) by replacing porosity and permeability with apparent porosity and apparent permeability. In other words, in general, the permeability deduced from the pressure-pulse decay method is an apparent permeability and the porosity used in calculation of permeability should be the apparent porosity. The conventional practice that uses porosity obtained from other methods may lead to significant errors in permeability, especially if the adsorption is significant.

With the apparent permeability, the Brace's solution can be written as

$$p_1 - p_f = \Delta p \frac{V_d}{V_u + V_d} e^{-\alpha t}, \tag{10}$$

in which

$$\alpha = \frac{k_a A}{c\mu L} \left(\frac{1}{V_u} + \frac{1}{V_d} \right), \tag{11}$$

where p_f is the final equilibrium pressure, Pa; Δp is the initial pressure difference, Pa; A is sample cross-sectional area, m²; and k_a is the apparent permeability (instead of permeability in original Brace's solution), m². Brace's solution [Eqs. (10) and (11)] is the first solution and its simplicity helped the pressure-pulse decay method to be widely used to measure the permeability of tight rock samples. However, the assumption of constant spatial pressure

gradient in the rock sample ($\frac{\partial p^2(x,t)}{\partial x^2} = 0$) may lead to significant permeability error in some cases which will be discussed later.

The more general Hsieh's solution (Hsieh et al. 1981) can be expressed in terms of dimensionless differential pressure as suggested by Dicker and Smits (1988) with modified symbols:

$$
\begin{aligned}
\Delta p_D &= \sum_{m=1}^{\infty} S_m \\
&= 2 \sum_{m=1}^{\infty} \exp\left(-t_D \theta_m^2\right) \frac{a\left(b^2 + \theta_m^2\right) - (-1)^m b\left[\left(a^2 + \theta_m^2\right)\left(b^2 + \theta_m^2\right)\right]^{0.5}}{\theta_m^4 + \theta_m^2\left(a + a^2 + b + b^2\right) + ab\left(a + b + ab\right)},
\end{aligned}
\tag{12}
$$

where S_m is the mth term; θ_m are the roots of Eq. (13); a and b are the ratios of apparent pore volume to upstream and downstream volume, respectively; t_D is dimensionless time, defined in Eq. (14); and Δp_D is the dimensionless pressure difference, defined in Eq. (15):

$$
\tan \theta = \frac{(a + b)\theta}{\theta^2 - ab},
\tag{13}
$$

$$
t_D = \frac{k_a t}{c \mu \phi_a L^2},
\tag{14}
$$

$$
\Delta p_D = \frac{p_1(t) - p_2(t)}{p_1(0) - p_2(0)},
\tag{15}
$$

where the apparent porosity, ϕ_a, and the apparent permeability, k_a, are used instead of the porosity and permeability used in the original solutions.

Although the analytical solution equation (12) is an exact solution of the problem including both an early time behavior and a late-time behavior, it is difficult to handle because of involving evaluation of infinite series. Therefore, the first term of Eq. (12) is often recommended for routine permeability calculation (Jones 1997), because the late-time solution is dominated by the first term (i.e., $m = 1$) in Eq. (12), as shown in Fig. 3. The other terms ($m > 1$) only significantly affect the solution at early time and cause the solution deviating from the linear line described by the first term in a semi-log plotting (Fig. 3). Such effects of the higher order terms on the solution decrease with decreasing of the parameter a (the ratio of pore volume in the sample over the volume of the upstream chamber, $a = b$ here). However, the solution itself does not tell how to distinguish the early time and the later time measurement data.
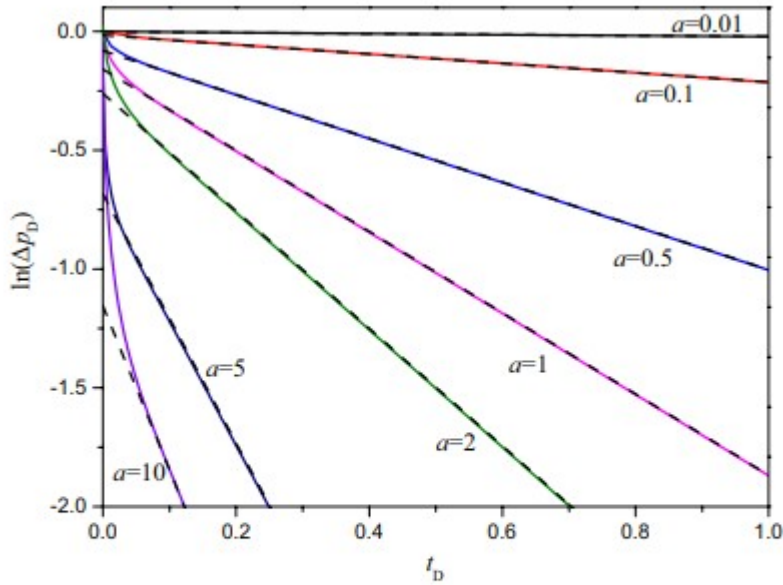
Fig. 3 Comparison of the general solution [Eq. (12), the solid curves] with the first term (the dashed curves) for different ratios of pore volume to chamber volume (assuming the volume of upstream chamber equals to that of the downstream chamber, i.e., $a = b$)

3 Numerical Analysis of Pressure-Pulse Propagation Process: Early and Later Time behaviors

As described in Fig. 1, the pressure-pulse decay method is basically an experiment of pressure-pulse propagation through the rock sample due to fluid flow from the upstream (higher pressure) chamber into the downstream (lower pressure) chamber. To understand the dynamics of such pressure-pulse propagation through the various rock samples under different experimental parameters, we performed numerical simulations of 18 cases that cover variations in typical rock properties and the experiment configurations (e.g., a and b). Table 2 shows the parameters used in these numerical simulations. Taking Case 1 as the base case, a series of numerical simulations are performed at varied values of chamber volumes (Case 2 through Case 5 for upstream chamber volumes and Case 6 through Case 8 for downstream chamber volumes), rock porosity (Case 9 through Case 11), permeability (Cases 12 and 13), adsorption parameters (Case 14 through Case 16), and slippage parameters (Cases 17 and 18) (Table 2). The initial pressure is set to 1 MPa and the pressure pulse is set to 0.1 MPa for all numerical tests. Note that Langmuir sorption model is used in Cases 14 to Case 16 to consider adsorption effects.

Numerical tests	V_u (cm^3)	V_d (cm^3)	ϕ	a	b	$k \times 10^{-18}$ (m^2)	m_L	p_L (MPa)	λ (MPa)
Case 1	98.2	98.2	0.05	0.1	0.1	1	–	–	–
Case 2	**982**	98.2	0.05	0.01	0.1	1	–	–	–
Case 3	**9.82**	98.2	0.05	1	0.1	1	–	–	–
Case 4	**4.91**	98.2	0.05	2	0.1	1	–	–	–
Case 5	**0.982**	98.2	0.05	10	0.1	1	–	–	–
Case 6	98.2	**982**	0.05	0.1	0.01	1	–	–	–
Case 7	98.2	**49.1**	0.05	0.1	0.2	1	–	–	–
Case 8	98.2	**9.82**	0.05	0.1	1	1	–	–	–
Case 9	98.2	98.2	**0.01**	0.02	0.02	1	–	–	–
Case 10	98.2	98.2	**0.1**	0.2	0.2	1	–	–	–
Case 11	98.2	98.2	**0.25**	0.5	0.5	1	–	–	–
Case 12	98.2	98.2	0.05	0.1	0.1	**0.01**	–	–	–
Case 13	98.2	98.2	0.05	0.1	0.1	**100**	–	–	–
Case 14	98.2	98.2	0.05	0.1	0.1	1	**0.001**	**5**	–
Case 15	98.2	98.2	0.05	0.1	0.1	1	**0.005**	**5**	–
Case 16	98.2	98.2	0.05	0.1	0.1	1	**0.01**	**5**	–
Case 17	98.2	98.2	0.05	0.1	0.1	1	–	–	**0.5**
Case 18	98.2	98.2	0.05	0.1	0.1	1	–	–	**1**

Table 2 Modeling parameters of numerical tests

The values given in bold are different from the corresponding values of the base case (Case 1)

In our numerical simulations, the core sample was discretized uniformly into 100 grid cells and two chambers were represented as two special grid cells attached to the upstream and downstream ends, respectively. The chamber grid cells have exact volumes as specified in each case with unit porosity and large permeability. The sample dimensions are representative of actual core tested in the laboratory flow tests, that is, 50 mm in diameter and 100 mm in length. CH_4 is used for the numerical simulations.

These simulations were completed using TOUGH + REALGASBRINE (TOUGH +), a widely used numerical simulator for non-isothermal multiphase flow (an aqueous phase and a real gas mixture) in a gas-bearing medium, with a particular focus in ultra-tight systems (Moridis and Pruess 2014). Different from the analytical solutions discussed above, TOUGH + model does not assume constant gas density, viscosity, and compressibility. Instead, these properties are functions of pressure and temperature based on the real gas EOS model implemented in TOUGH + . Therefore, they will vary with space in the rock sample following the pressure as in reality, although such variations are expected to be small for the given pressure difference in typical pressure-pulse decay experiments. In addition, TOUGH + adopts instant equilibrium adsorption/desorption (e.g., Langmuir model). Fewer simplifications make the numerical simulator to be more suitable than the analytical solutions to understand the dynamics and mechanism of the pressure-pulse propagation taking placing in a pressure-pulse decay experiment.

Figure 4 shows semi-log plotting of dimensionless pressure difference vs. dimensionless time for all cases. In general, the dimensionless pressure-difference decays quickly at early time and then approaches exponentially

decay mode of dimensionless time (shown as straight lines in the plotting) after certain timepoint, although the slope may vary greatly between cases.
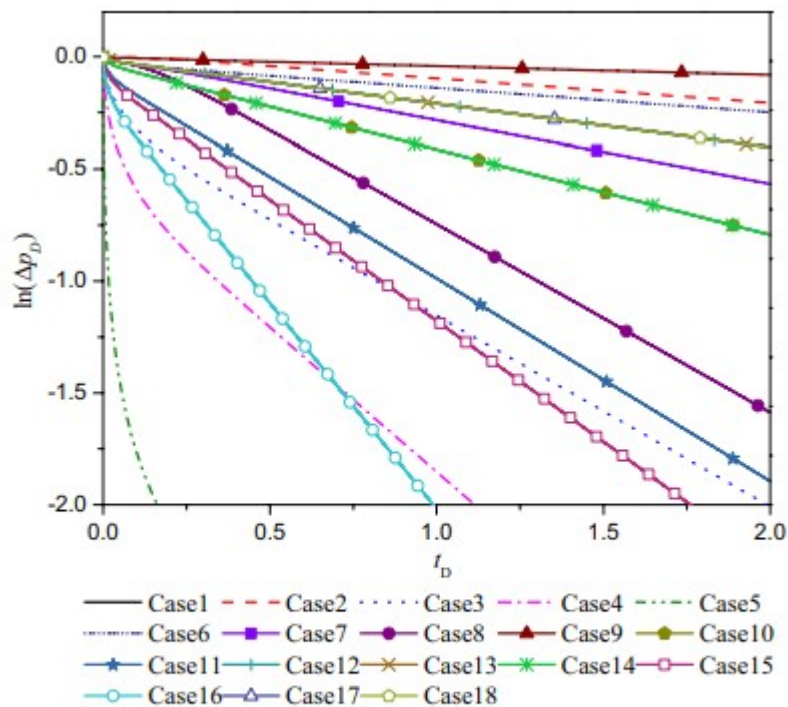

Fig. 4 Pressure responses in various cases (Case 1 is overlapped by the Cases 12, 13, 17, and 18, so that the black for Case 1 cannot be seen)

To understand the mechanism behind such big changes in pressure decay pattern between early time and later time, we plot the contour of the normalized pressure change (defined as $\frac{p(x,t)-p(x,0)}{p(0,0)-p(L,0)}$) in temporal and spatial domain in Fig. 5 to see what happens inside the rock sample during the experiment. Each figure shows the evolution of pressure profile within the rock sample over time for each case. Breakthrough curve (the dashed line in Fig. 5) is defined as the normalized pressure reaches to 0.005 to describe the position of the front of the pressure pulse in the rock sample. In general, for the given pressure difference, velocity of the pulse propagation would be proportional to the permeability of the rock but inversely proportional to the storage terms (e.g., the pore volume of the rock, adsorption capability, and the fluid compressibility). For example, with two orders increases in permeability among Cases 1, 12, and 13, the breakthrough time decreases from 65530 s to 510 s to 7 s, respectively, in the same orders of the permeability. While the porosity increases from 0.01 to 0.05, 0.1 and finally to 0.25, the breakthrough time increases from 120 s to 510 s, 1010 s and finally to 2010 s, almost in the same multiple growths of the porosity. The

effects of adsorption and slippage on breakthrough time are similar to the results of porosity and permeability due to the changes of apparent porosity and apparent permeability. Another important factor is upstream chamber volumes. For example, the breakthrough time is about 510 s in Case 1, 900 s in Case 4, and 2370 s in Case 5, as the upstream chamber volume decreases from 98.2 to 4.91, to 0.982 cm^3, respectively. This is because a larger upstream chamber can hold more gas at the given pressure than a smaller one, so that its pressure drop due to the same amount of gas loss to the rock sample tends to be smaller. As a result, a larger upstream chamber can keep a larger driving force for flow through the rock sample, which results in fast breakthrough of the pressure pulse. The downstream volume has little effects on the breakthrough time (Cases 6 through Case 8), because the downstream chamber has no effects on the pressure-pulse propagation before the pressure pulse breakthrough the rock sample.
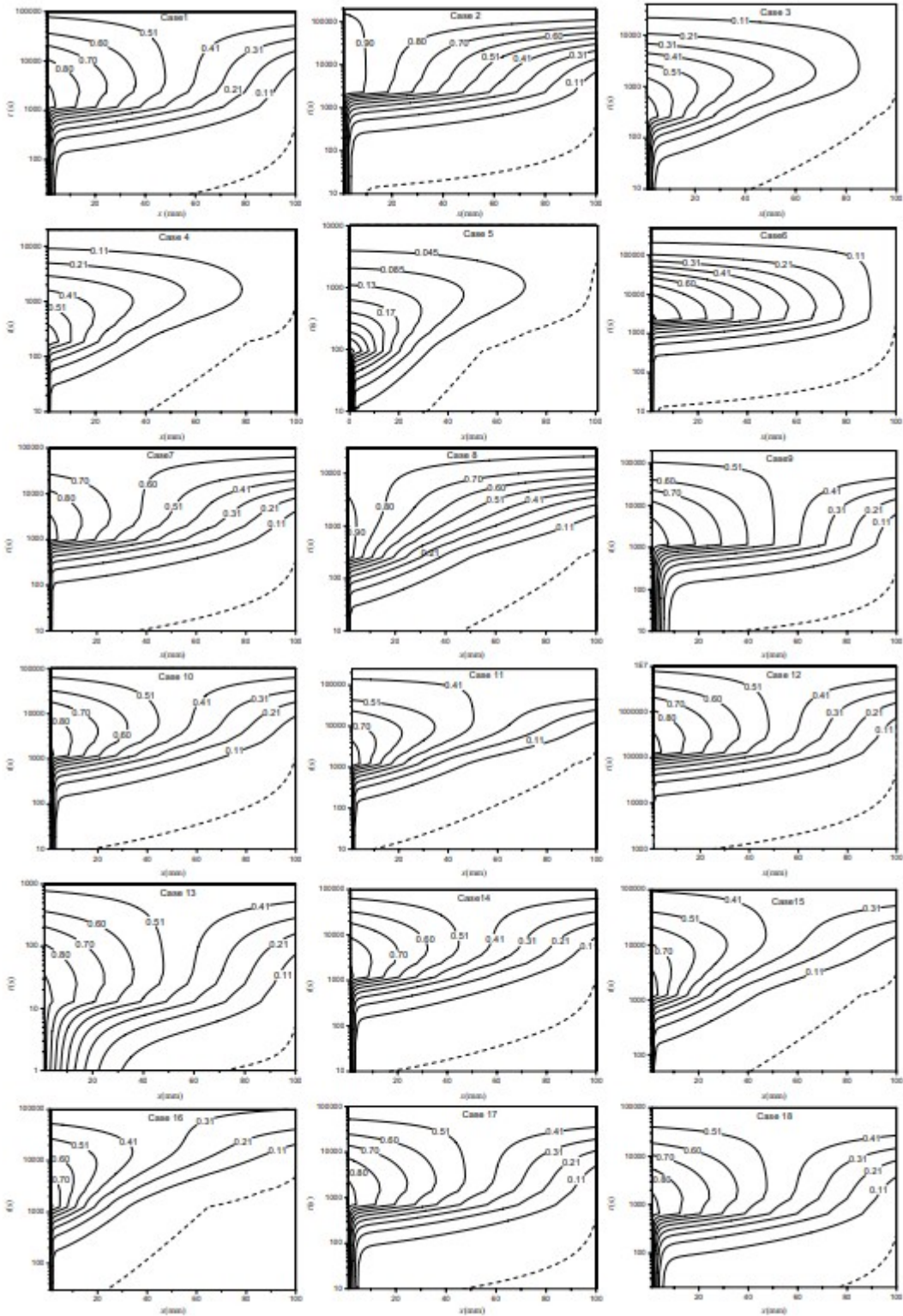
Fig. 5 Contours of the normalized pressure change in space and dimensionless time domain for Cases 1–18. The dashed lines describe the breakthrough curve

The physical process of the pressure-pulse propagation is different before and after the breakthrough time. Before that time, the dissipation of the

pressure at the upstream chamber behaves as if the pressure pulse is propagating through an infinite medium, which is quite different from the situation after the pressure pulse reaches the downstream chamber, so that the downstream boundary starts to affect the process. This difference in the process of the pressure-pulse propagation results in different behaviors of the measured pressure response (usually expressed as pressure difference between the upstream and downstream chambers) at early time and later time. The turning point is the time the pressure pulse reaches the downstream end. After that breakthrough time, the flow becomes "quasi-steady", in which the pressure distributions within the rock quickly approach the constant gradient patterns (Hsieh et al. 1981).

To further show the evolution of pressure gradient over time, we plotted the difference in pressure gradient at two ends of the rock sample (Fig. 6). In principle, this difference shall be the maximum at time zero, gradually decreases with time and finally reaches zero, because the system reaches the equilibrium state (e.g., Fig. 6a). As shown in Fig. 6b, although the pressure gradient difference decreases in quite a different rate among different cases, it approaches zero (< 0.005) for all cases when $t_D > 0.4$. Furthermore, we calculated the contribution η [defined as

$$\eta = S_1 / \sum_{m=1}^{\infty} S_m$$

, where S_m is the mth in Eq. (12)] of the first term in Eq. (12) to all terms when $t_D = 0.4$ at different values of a and b, as shown in Fig. 7. As can be seen from the figure, the first term (late-time solution) contributes more than 99.7% for all cases when $t_D = 0.4$, indicating that the early time data can be neglected after $t_D > 0.4$. Therefore, $t_D > 0.4$ can be seen as a safe criterion for selecting the later time measurements. However, this criterion is not practical, because the dimensionless time, t_D, contains the unknown permeability as defined in Eq. (14). We have to find a new criterion that is independent of permeability, which we will discuss next.
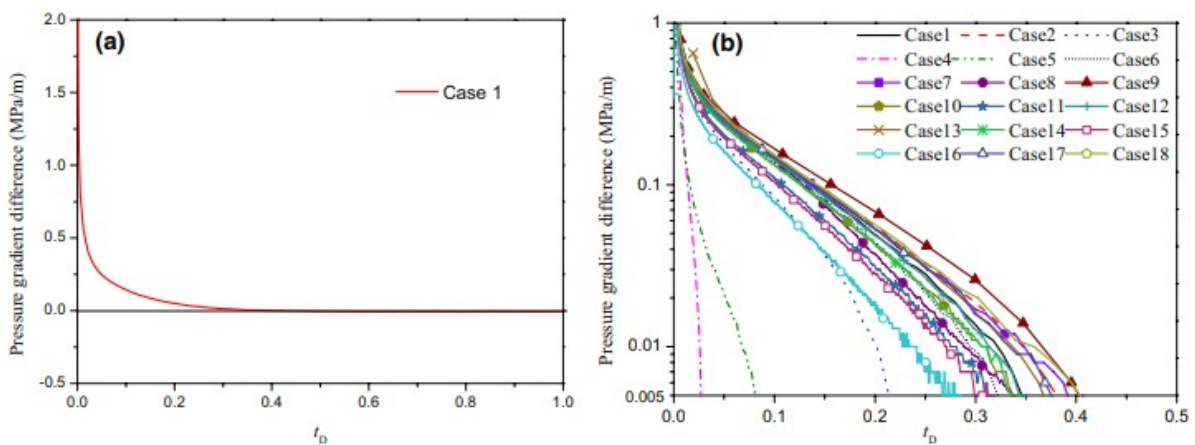

Fig. 6 Pressure gradient difference between two ends of the rock sample: **a** Case 1 and **b** Cases 1–18
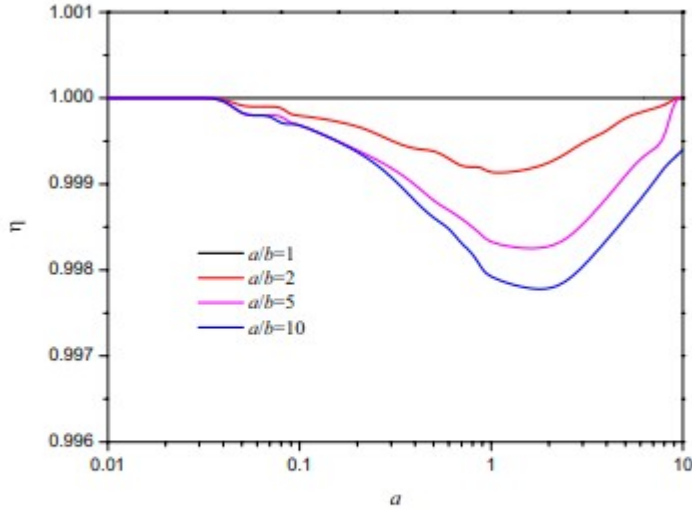
Fig. 7 Contribution of the first term in Eq. (12) to all terms when $t_D = 0.4$

4 A new Approach to Determine Permeability, Porosity, and Adsorption Capacity

4.1 Determination of Apparent Porosity

As discussed earlier, the first step to determine accurate permeability from a pressure-pulse decay experiment is to obtain the consistent apparent porosity which may vary with tested rock, type of working gas, and other experiment settings. We use the Boyle's law to estimate the apparent porosity of a rock sample from the mass balance equation at end of the given pressure-pulse experiment:

$$\frac{V_u\,(p_0 + \Delta p)}{z_{p_0 + \Delta p}} + \frac{(V_d + \phi_a A L)\, p_0}{z_{p_0}} = \frac{(V_u + V_d + \phi_a A L)\, p_f}{z_{p_f}}, \tag{16}$$

where z is gas compressibility factor at given pressure ($= 1$ for ideal gas) and p_f is the final pressure at end of pressure-pulse experiment. A is the cross-sectional area and L is the length of the rock sample. The apparent porosity can be easily solved from algebra equation (16), since all other parameters are known.

4.2 Determination of Apparent Permeability with Later Time Data

Although we understand that the time of the pressure-pulse breakthrough is the turning point between the early time and later time pressure responses and that the pressure gradient within the rock samples becomes almost spatially independent after $t_D = 0.4$ (Fig. 6), the criterion in terms of t_D cannot be used directly to distinguish the early time and later time data in pressure decay method, because t_D itself contains the unknown permeability which needs to be inferred from the measured data. To overcome this difficulty,

inspired by Eq. (12), we propose to define a new scaled pressure decay, $p*$, as follows:

$$p^* = \frac{1}{\theta_1^2} \ln \frac{2C_1}{\Delta p_D}, \tag{17}$$

In which

$$C_1 = \frac{a\left(b^2 + \theta_1^2\right) + b\left[\left(a^2 + \theta_1^2\right)\left(b^2 + \theta_1^2\right)\right]^{0.5}}{\theta_1^4 + \theta_1^2\left(a + a^2 + b + b^2\right) + ab\left(a + b + ab\right)}. \tag{18}$$

Considering that the first term of the general analytical solution equation (12) is a good approximation solution for later time as discussed before, we have the later time solution as below:

$$\Delta p_D = 2C_1 \exp\left(-t_D \theta_1^2\right). \tag{19}$$

By inserting Eq. (17) into Eq. (19), we simply have

$$p^* = t_D. \tag{20}$$

In other words, the scaled decay curve, $p^*(t_D)$, is a 1:1 straight line in later time. Therefore, we can conveniently use $p^* > 0.4$ as the criterion to differentiate the early time data and late later data in pressure-pulse tests. We re-plot the data of Fig. 4 in Fig. 8 in terms of p^* vs. t_D. As shown in Fig. 8, although p^* can be positive or negative at early time depending on chamber volume ratio (e.g., negative for cases with $V_u > V_d$ and positive otherwise), all data are nicely scaled to the single 1:1 straight line after $t_D > 0.4$ (or $p^* > 0.4$). The neat thing is that p^* is independent of the unknown permeability. Therefore, the criterion base on p^* is more practical than that based on t_D.

Fig. 8 Relationship of scaled pressure decay and dimension-less time for Cases 1–18
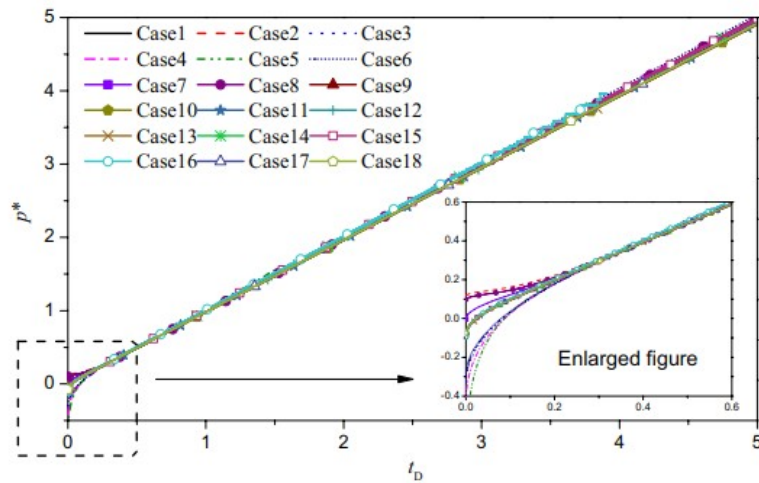
Furthermore, by defining a scaled time

$$t^* = \frac{t}{c\mu\phi_a L^2},$$

(21)

we can rewrite Eq. (20), using Eq. (14), as

$$p^* = k_a t^*.$$

(22)

Therefore, the apparent permeability can be calculated from Eq. (22). The procedure to process the measured data series $\{\Delta p_i, t_i\}$ can be summarized as follows:

Step 1 Calculate apparent porosity by solving Eq. (16).

Step 2 Calculate $p*_ipi*$ using Eq. (17); $t*_iti*$ using Eq. (21).

Step 3 Calculate the raw estimation of permeability, $k_i = \frac{p_i^*}{t_i^*}$ if $p_i^* > 0.4.$

Step 4 Calculate the mean and the standard deviation of estimated permeability $\{k_i\}$.

A list of source code implementing this algorithm in MATLAB is provided in "Appendix". We note that there are other methods available for obtaining the permeability from the measured data series $\{\Delta p_i, t_i\}$. One such technique would be the linear regression. No attempts have been made to examine the rigor or nuances of those methods.

4.3 Adsorption and Slippage

The adsorption and slippage parameters can also be inferred from a set of pressure-pulse decay experiments. First, the true porosity could be measured using non-adsorption gas or other independent porosity measurement methods under the same effective stress, and then, the equivalent porosity due to adsorption can be easily calculated using Eq. (6). Therefore, if the experiments are performed at two or more final pore pressures, but the same effective stress, the common equilibrium adsorption models, and corresponding parameters (e.g., Langmuir model, Freundlich model, D–A model, and BET model) can be deduced readily using Eq. (7).

After obtaining apparent permeabilities under two or more pore pressure with the same effective stress, the slippage parameter and true permeability can also be determined using Eq. (2).

4.4 Verification of the Proposed Method

To verify the accuracy of the proposed method, we calculated the parameters, using the method described in Sects. 4.2 and 4.3, from the simulated pressure decay data of 18 cases described in Sect. 3, and then compare them to the parameters actually used in the numerical simulations (Tables 3 and 4).

Table 3 Calculated permeabilities and the true value (Case 1–Case 13)

	True permeability (10^{-18} m^2)	Brace's method		Cui's method		The proposed method		
		k (10^{-18} m^2)	Relative error (%)	k (10^{-18} m^2)	Relative error (%)	k (10^{-18} m^2)	Relative error (%)	Standard deviation (10^{-18} m^2)
Case 1	1	0.981	− 1.9	0.998	− 0.2	0.997	− 0.3	0.0035
Case 2	1	0.967	− 3.3	0.994	− 0.6	0.999	− 0.1	0.0099
Case 3	1	0.815	− 18.5	1.039	3.9	0.995	− 0.5	0.0050
Case 4	1	0.674	− 32.6	1.088	8.8	1.012	1.2	0.0063
Case 5	1	0.275	− 72.5	1.251	25.1	1.007	0.7	0.0032
Case 6	1	0.975	− 2.5	1.002	0.2	1.010	1.0	0.0137
Case 7	1	0.962	− 3.8	0.978	− 2.2	0.991	− 0.9	0.0052
Case 8	1	0.766	− 23.4	0.975	− 2.5	0.998	− 0.2	0.0041
Case 9	1	0.993	− 0.7	0.996	− 0.4	0.997	− 0.3	0.0021
Case 10	1	0.964	− 3.6	0.997	− 0.3	0.997	− 0.3	0.0022
Case 11	1	0.921	− 7.9	0.998	− 0.2	0.997	− 0.3	0.0023
Case 12	0.01	0.981	− 1.9	0.00998	− 0.2	0.00997	− 0.3	0.000027
Case 13	100	0.981	− 1.87	99.8	− 0.2	99.6	− 0.4	0.539

Table 4 Comparison between the calculated parameters and the true values in cases with adsorption

	True permeability (10^{-18} m^2)	Brace's method		Cui's method		The proposed method			
		k (10^{-18} m^2)	Relative error (%)	k (10^{-18} m^2)	Relative error (%)	k (10^{-18} m^2)	Relative error (%)	m_L	p_L (MPa)
Case 14	1	0.965	− 3.5	0.997	− 0.3	0.997	− 0.3	0.0009	4.95
Case 15	1	0.906	− 9.4	1.001	0.1	0.998	− 0.2	0.0049	4.86
Case 16	1	0.841	− 15.9	1.009	0.9	1.008	0.8	0.0099	4.82

Table 3 shows the comparison between the calculated permeability using the proposed method from the data generated by numerical simulations (Case 1 through Case 13) and the true values used in numerical simulation. For comparison, we also included the estimated permeability from the same data sets using the methods from Brace et al. (1968) and Cui et al. (2009). As shown in Table 3, the proposed method successfully estimated the permeability. The determined permeability values are very close to the true values. The relative error between the mean estimated value and the true value ranges from 0.1 to 1.2%. The calculated standard deviation is within 1.37% of the true value.

The calculated permeability using Cui's method is close to the true value for most cases. Since Cui's method does not differentiate the early time and late-time data, large error can also be found in some cases, especially for cases with lager value of a (e.g., the relative error is 8.8% in Case 4 for $a = 2$, and 25.1% in Case 5 for $a = 10$), in which the early time data deviate the single-exponential behavior significantly. An accurate estimation of permeability can improve the prediction of hydrocarbon in-place and recovery. Roadifer and Scheihing (2011) have taken the example of an actual field reservoir and demonstrate that a permeability error of 20% can propagate throughout the model building and history matching process, and may cause 27.8% underestimation of oil recovery.

On the other hand, the permeability estimated by the Brace's method is close to the true value only if the volume ratios, *a* and *b*, are small (Case 9). When the volume ratios are large, the Brace's method can significantly underestimate permeability and the relative error can reach up to 72.5% (Case 5).

Table 4 shows the permeability results for the cases with adsorption effects. The permeability will be underestimated when testing sorptive rocks using Brace's solution even for cases with small volume ratios. Such trend is in qualitative agreement with the experimental results in Wang et al. (2015) and Feng et al. (2016). These larger errors in estimated permeability are caused by two reasons: (1) violations of the strict assumptions used in developing Brace's solution and (2) error in porosity on permeability estimation (the apparent porosity rather than true porosity should be used). On the other hand, the results of using Cui's method and our method match the true permeability very well, with maximum relative errors of 0.8% in our method and 0.9% in Cui's method. It is worth mentioning that in Cui's method, the adsorption model and parameters are assumed to be known accurately, which requires additional adsorption experiments to obtain apparent porosity and only limits to Langmuir model. While for other adsorption models, permeability error can also be induced. For example, we carried out additional numerical cases using similar parameters as Case 14 but replacing Langmuir model with Freundlich model ($\psi(p)=0.01p0.2\psi(p)=0.01p0.2$) to generate pressure decay data. It turns out that a permeability error of 9.3% is produced by Cui's method. However, only a permeability error of 0.6% is caused with our method. Note that, in our method, the apparent porosity is estimated based on Eq. (16) without assuming any particular adsorption model.

The adsorption parameters were calculated by solving Eq. (8b) using two apparent porosity values obtained from two sets of simulations with initial pressure at 1 MPa and 2 MPa, respectively, for Cases 14–16. The calculated parameters match the true Langmuir parameters used in the numerical simulations very well (Table 4), supporting the usefulness of our method.

Table 5 shows the results of the cases with gas-slippage effects. The slippage parameter λ and absolute permeability were calculated using Eq. (2) using the apparent permeabilities obtained from two sets of simulations of Cases 17 and 18 with initial pressure at 1 MPa and 2 MPa, respectively. As listed in Table 5, the slippage parameter determined is nearly identical to the true values (Table 2). The apparent permeability increases with slippage effects for a given pressure.

Table 5 Permeability results of numerical tests with gas-slippage effects

Numerical tests	True permeability $(10^{-18}\,m^2)$	Apparent permeability $(10^{-18}\,m^2)$	Absolute permeability $(10^{-18}\,m^2)$	Standard deviation $(10^{-18}\,m^2)$	λ
Case 17	1	1.4722	1.012	0.0073	0.48
Case 18	1	1.9473	1.013	0.0103	0.97

To sum up, there are three main differences between our method and Brace's, Cui's method. First, the proposed method defines a new dimensionless pressure that allows consistent separation of the early and late-time regimes, which is lack in Brace's and Cui's method. Second, in Cui's method, the apparent porosity is calculated with the known Langmuir isotherm model to remove the effects of the adsorption on the determination of the permeability. In our method, the apparent porosity is measured from the same pressure-pulse tests using the initial pressure and final pressure, which is independent of particular adsorption models. Furthermore, with our method, we could not only remove the effects of the adsorption on the determination of the permeability, but also could identify proper adsorption model and parameters with multiple pressure-pulse tests. Third, the idea or method to simultaneously determine permeability, porosity, adsorption model/parameters, and slippage parameters from pressure-pulse decay experiments is novel.

5 Application to Real Measurements

In this section, we applied the proposed method to process the real measured data under various experiment setting including different gas types. Two sets of pressure-pulse decay experiments with different volume ratios were carried out. Test 1 was conducted on a sorptive rock, shale, at constant effective stress of 3 MPa by fixing the difference between the confining pressure (p_c) and the pore pressure (p). In this test, two types of gases (CH_4 and He) were used, respectively, among which CH_4 is found to be adsorbed by the shale. Test 2 was conducted on a rock-like sample (a mixture of ordinary Portland cement, sand, and water at a ratio of 1:1.2:0.65) at a constant pore pressure of 2 MPa but the confining pressures p_c ranges from 5 to 20 MPa, resulting in the effective stress varying from 3 to 18 MPa. Only He was used in Test 2. The purity of gases used in these experiments (He and CH_4) was 99.999%. The detailed experimental schemes are listed in Table 6.

Table 6 Experimental schemes and results of Test 1 and Test 2

	Fluid	p_c (MPa)	p (MPa)	ϕ_a (%)	k_a (m^2)
Test 1	He	5	2	2.08	$1.594 \pm 0.044 \times 10^{-18}$
		6.5	3.5	2.01	$1.494 \pm 0.039 \times 10^{-18}$
		8	5	2.14	$1.447 \pm 0.038 \times 10^{-18}$
		9.5	6.5	1.89	$1.436 \pm 0.087 \times 10^{-18}$
	CH$_4$	5	2	6.02	$1.601 \pm 0.075 \times 10^{-1} \pm^8$
		6.5	3.5	4.83	$1.557 \pm 0.068 \times 10^{-18}$
		8	5	4.05	$1.515 \pm 0.057 \times 10^{-18}$
		9.5	6.5	3.53	$1.498 \pm 0.080 \times 10^{-18}$
Test 2	He	5	2	24.03	$7.372 \pm 0.019 \times 10^{-17}$
		10	2	21.87	$4.525 \pm 0.036 \times 10^{-17}$
		15	2	20.94	$3.061 \pm 0.023 \times 10^{-17}$
		20	2	20.46	$2.306 \pm 0.041 \times 10^{-17}$

The estimated permeability (with its standard deviation) and porosity of the samples are shown in Table 6. As expected, the apparent permeability in Test 1 is nearly identical for all cases, since the effective stress is constant, although the gas-slippage effect slightly modifies the apparent permeability under the different pore pressure. The estimated slippage parameter λ is 0.34 for He and 0.20 for CH$_4$ and the true average permeability is 1.41×10^{-18} m^2. The apparent porosity in Test 1 with He shows little changes with the pore pressure (under the same effective stress), implying that He is not adsorbed by the shale. Therefore, the difference in the apparent porosity of the shale sample obtained with CH$_4$ and He can be seen as a measurement of the equivalent porosity due to adsorption of CH$_4$ by the shale. Given the relationship between the equivalent porosity due to adsorption and the associated pore pressure, we can easily obtain the adsorption model and corresponding parameters. Figure 9 shows the fitting curve of experimental data using different sorption models. The fitted parameters for these sorption models are listed in Table 7. Note that the experimental temperature was above methane's critical temperature ($-$ 82.7 °C); hence, the pseudo-saturation vapor pressure (Agarwal and Schwartz 1988; Harpalani et al. 2006) was used and calculated in BET model and D–A model. The figure indicates that Langmuir modeled results show the best match with the experimental results (with R^2 value of 0.99). Compared to other sorption models, BET model has the poorest performance with R^2 smaller than 0.5. Moreover, independent adsorption experiments were conducted on shale sample to measure adsorption parameters, which gives the Langmuir parameters $m_L = 0.0014$ and $p_L = 5.67$ MPa, matching the calculated results (Table 7) well. This proves that the proposed simultaneously determination of permeability, porosity, and adsorption capacity is effective.
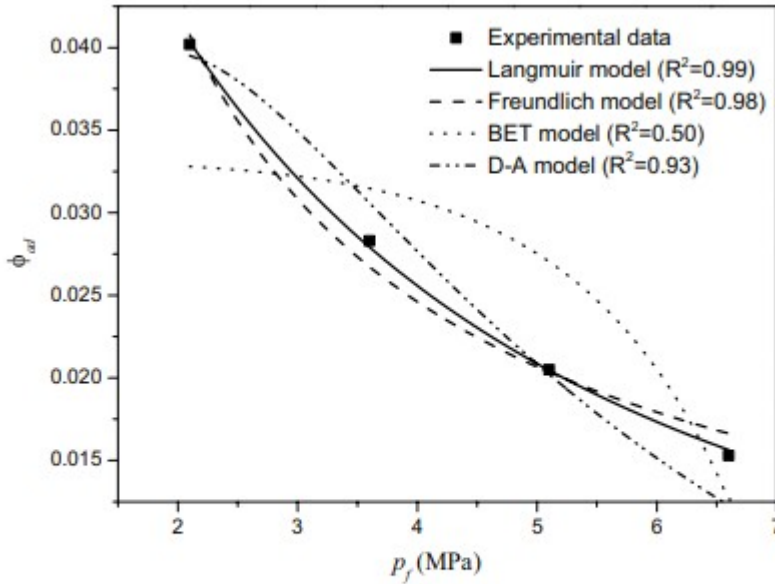
Fig. 9 Fitting curve of experimental data using different sorption models (derivative function of sorption models are used to fitting experimental data)

**Table 7** Modeled parameters for different sorption models

Sorption model	Function	Modeled parameters	R^2
Langmuir model	$\psi(p) = \frac{m_L p}{p_L + p}$	$m_L = 0.0011$; $p_L = 5.32$ MPa	0.99
Freundlich model	$\psi(p) = K p^n$	$K = 8.62 \times 10^{-4}$; $n = 0.217$	0.98
BET model	$\frac{1}{\psi(p)(p_0/p - 1)} = \frac{1}{V_m C} + \frac{C-1}{V_m C} \frac{p}{p_0}$	$V_m = 0.0013$; $C = 0.763$	0.50
D–A model	$\psi(p) = V_0 \exp\left[-D\left\{\ln\left(\frac{p_0}{p}\right)^2\right\}\right]$	$V_0 = 5.00 \times 10^{-4}$; $D = 0.439$	0.93

Note that p_0 is the saturation vapor pressure in BET model and D–A model

Both the permeability and the porosity in Test 2 decrease with the increase of confining pressure for fixed pore pressure. This is consistent with the theory of the general relationship between the rock porosity/permeability and the effective stress. Because only one gas (non-adsorptive He) and a single pore pressure were used in Test 2, we could not infer the parameters of slippage and adsorption from these measurements.

Finally, with the obtained apparent porosities and permeabilities, the curves of p^* vs. t_D are plotted in Fig. 10. The figure clearly illustrates that all data from these experiments (after $p^* > 0.4$) obey Eq. (20), the general later time scaled solution.

Fig. 10 Relationship of scaled pressure decay and dimensionless time for Test 1 and Test 2
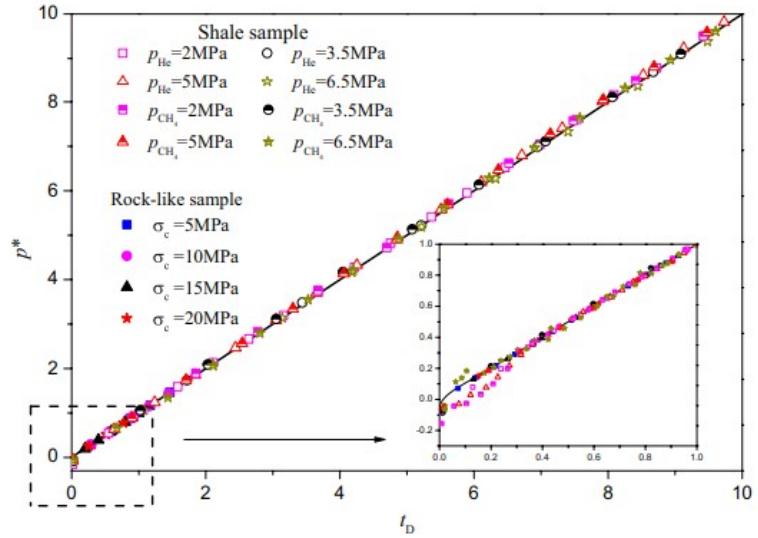
To validate the accuracy of the obtained parameters from experimental tests, these obtained parameters (permeability, porosity, adsorption, and slippage parameters) were used as input for the numerical model to simulate the given pressure-pulse decay experiments. Figure 11 shows the simulated upstream and downstream pressures compared against the measured values for one of the cases (CH_4 pressure of 2 MPa in Test 1), as listed in Table 6 (others are similar). As can be seen from the figure, the solid curves match the solid circles very well, indicating that the parameters of the rock sample (permeability, porosity, adsorption, and slippage parameter) obtained using the proposed method are correct.
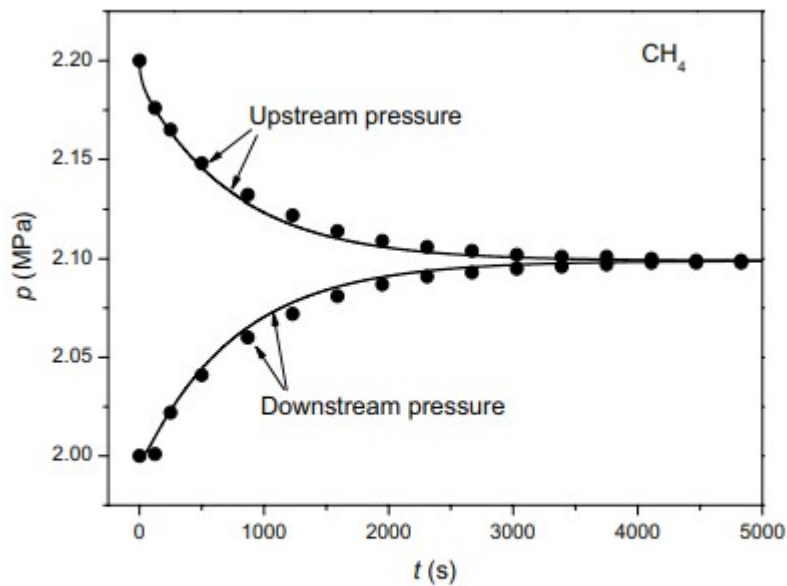
Fig. 11 Pressure responses in the upstream chamber and downstream chamber generated from numerical test (solid curves) and experimental test for the CH$_4$ pressure of 2 MPa in Test 1 (solid circles)

6 Conclusions

The pressure-pulse decay method can be seen as an experiment of the pressure-pulse propagation through the rock sample. The different flow conditions before and after the breakthrough of the pressure pulse result in different behaviors in terms of the observed pressure-pulse decay curve, i.e., early time decay curve (before breakthrough) and later time decay curve (after breakthrough). With our new scaling method, the later time decay curves obtained from experiments with various rock properties and experiment setting parameters can be scaled into a single straight 1:1 line on a $p^*(t_D)$ plot (scaled decay vs. dimensionless time plot). It was found that $p^* > 0.4$ could be the universal criterion for determining the later time decay data used to estimate the permeability for all typical types of rock, gas, and experimental devices. Unlike the previous similar criterion for determining later time decay data in the literature, this criterion does not depend on the unknown permeability, so that it can be easily used to automatically distinguish the later time data from the raw measurements.

Thoroughly analysis of the governing equations reveals that the permeability and the porosity controlling the pressure propagation in the rock are often apparent values if adsorption and gas slippage are existing (e.g., in shale gas applications). Therefore, the value directly estimated from pressure decay method is the apparent permeability, while the apparent porosity (i.e., including the adsorption-induced storage) must be used in calculation of such apparent permeability. We proposed a method to estimate the

apparent porosity based on the mass balance equation in terms of initial pressure and final pressure of the same pressure-pulse decay experiment for determining permeability. The equivalent porosity of the rock sample due to adsorption can be further obtained if either the true porosity is known independently or a non-adsorptive gas is also used under the same experimental conditions. Furthermore, the adsorption model and corresponding parameters can be estimated from a set of pressure-pulse decay experiments including different pore pressure, but the same effective stress. In later case, the slippage parameter can also be inferred from the pressure-pulse decay experiments.

Based on the findings above, a new robust approach to simultaneously determine permeability and porosity from pressure–pulse decay measurements is developed. The new approach is implemented into MATLAB to automatically process the pressure-pulse decay data and estimate the apparent permeability including its standard deviation and the apparent porosity of rock samples. The tests of the method on the pressure-pulse decay data obtained by numerical experiments using TOUGH + REALGASBRINE prove that the proposed approach can provide permeability, porosity, adsorption parameters, and slippage parameter that are very close to the true values (the input values used in numerical simulations) without limitation of particular adsorption models. We also demonstrated the successful applications of the proposed approach to the real experimental data involving two rock types, two gas types, and various pore and confining pressures.

Acknowledgements

Appendix

The main MATLAB code implemented for permeability and porosity calculation for pressure-pulse decay test is shown as below.

```matlab
clear all;clc;
[Vu,Vd,A,l,p0,pf,dp,u,c,z1,z2]=textread('parameter.txt','%f%f%f%f%f%f%f%f%f%f%f', 'delimiter', ',') % please
input the value of upstream and downstream chamber volume(Vu, Vd), rock size (A,l), initial pressure (p0), final
equilibrium pressure (pf), pulse pressure (dp), fluid viscosity (u), fluid compressibility (c) and deviation factor of gas
(z1 and z2) in a separated file named "parameter.txt". SI Units should be used.

Poro=-((Vu*dp+p0*(Vd+Vu))/z1-(pf*(Vd+Vu))/z2)/((A*l*p0)/z1-(A*l*pf)/z2); % porosity calculation
a=Poro*A*l/Vu % Volume ratio of pore to upstream
b=Poro*A*l/Vd % Volume ratio of pore to downstream

syms x
f1=tan(x)-(a+b)*x./(x.^2-a*b);
f11=matlabFunction(f1);
theta=fsolve(@(x)[f11(x)],1); % The first root of Eq.(13)
C1=(a*(b^2+(theta)^2)-(-
1)^1*b*sqrt((a^2+(theta)^2)*(b^2+(theta)^2)))/((theta)^4+(theta)^2*(a+a^2+b+b^2)+a*b*(a+b+a*b));

[t p]=textread('pressuredata.txt') %  please input measured data of time and differential pressure in a separated file
named "pressuredata.txt"
pd=p/dp% Dimensionless pressure
ps=1/theta^2*log(2*C1)-1/theta^2*log(pd) % scaled pressure decay
ts=t/l^2/(Poro)/u/c %

% permeability calculation
n=size(ps,1) % cycle index
j=1
for i=1:n
    if(ps(i)>0.4) % The early time data are skipped here.
        k(j)=ps(i)/ts(i)
        j=j+1
        end
end
km=mean(mean(k)) % avarage value permeability
kvar=var(k) % The variance of permeability
kstd=std(k) % The standard deviation of permeability
fprintf('Permeability= %e \n',km)
fprintf('Standard deviation of permeability= %e \n',kstd)
```

References

Agarwal RK, Schwartz JA (1988) Analysis of high-pressure adsorption of gases on activated carbon by potential theory. Carbon 26(6):873–887. https://doi.org/10.1016/0008-6223(88)90111-X

Berlepsch TV, Haverkamp B (2016) Salt as a host rock for the geological repository for nuclear waste. Elements 12(4):257–262. https://doi.org/10.2113/gselements.12.4.257

Brace WF, Walsh JB, Frangos WT (1968) Permeability of granite under high pressure. J Geophys Res 73:2225–2236. https://doi.org/10.1029/JB073i006p02225

Chen T, Stagg PW (1984) Semilog analysis of the pulse-decay technique of permeability measurement. Soc Pet Eng J 24:639–642. https://doi.org/10.2118/11818-PA

Cui X, Bustin AMM, Bustin RM (2009) Measurements of gas permeability and diffusivity of tight reservoir rocks: different approaches and their applications. Geofluids 9:208–223. https://doi.org/10.1111/j.1468-8123.2009.00244.x

Dicker A, Smits R (1988) A practical approach for determining permeability from laboratory pressure-pulse decay measurements. In: International Meeting on Petroleum Engineering. Society of Petroleum Engineers. https://doi.org/10.2118/17578-MS

Duong DD (1998) Adsorption analysis: equilibria and kinetics. Imperial College Press, London

Fei Y, Johnson RL Jr, Gonzalez M, Haghighi M, Pokalai K (2018) Experimental and numerical investigation into nano-stabilized foams in low permeability reservoir hydraulic fracturing applications. Fuel 213:133–143. https://doi.org/10.1016/j.fuel.2017

Feng R (2017) An optimized transient technique and flow modeling for laboratory permeability measurements of unconventional gas reservoirs with tight structure. J Nat Gas Sci Eng 46:603–614. https://doi.org/10.1016/j.jngse.2017.08.032

Feng R, Harpalani S, Pandey R (2016) Evaluation of various pulse-decay laboratory permeability measurement techniques for highly stressed coals. Rock Mech Rock Eng 50:297–308. https://doi.org/10.1007/s00603-016-1109-7

Feng R, Liu J, Harpalani S (2017) Optimized pressure pulse-decay method for laboratory estimation of gas permeability of sorptive reservoirs: part 1-background and numerical analysis. Fuel 191:555–564. https://doi.org/10.1016/j.fuel.2016.11.079

Hannon MJ (2016) Alternative approaches for transient-flow laboratory-scale permeametry. Transp Porous Med 114(3):719–746. https://doi.org/10.1007/s11242-016-0741-8

Harpalani S, Prusty BK, Dutta P (2006) Methane/CO2 sorption modeling for coalbed methane production and CO2 sequestration. Energy Fuels 20(4):1591–1599. https://doi.org/10.1021/ef050434l

He J, Ling K (2016) Measuring permeabilities of Middle–Bakken samples using three different methods. J Nat Gas Sci Eng 31:28–38. https://doi.org/10.1016/j.jngse.2016.03.007

Hsieh P, Tracy J, Neuzil C, Bredehoeft J, Silliman S (1981) A transient laboratory method for determining the hydraulic properties of 'tight' rocks-I. Theory. Int J Rock Mech Min Sci Geomech Abstr 18:245–252. https://doi.org/10.1016/0148-9062(81)90979-7

Jin L, Hawthorne SB, Sorensen JA, Pekot LJ, Kurz BA, Smith SA, Heebink LV, Herdegen V, Bosshart NW, Torres Rivero JA, Dalkhaa C (2017) Advancing

CO2 enhanced oil recovery and storage in unconventional oil play-experimental studies on Bakken shales. Appl Energy 208:171–183. https://doi.org/10.1016/j.apenergy.2017.10.054

Jones SC (1997) A technique for faster pulse-decay permeability measurements in tight rocks. SPE Form Eval 12:19–26. https://doi.org/10.2118/28450-PA

Kamath J, Boyer R, Nakagawa F (1992) Characterization of core scale heterogeneities using laboratory pressure transients. SPE Form Eval 7:219–227. https://doi.org/10.2118/20575-PA

Karacan CÖ (2008) Evaluation of the relative importance of coal bed reservoir parameters for prediction of methane inflow rates during mining of longwall development entries. Comput Geosci 34(9):1093–1114. https://doi.org/10.1016/j.cageo.2007.04.008

Kim TH, Cho J, Lee KS (2017) Evaluation of CO2 injection in shale gas reservoirs with multi-component transport and geomechanical effects. Appl Energy 190:1195–1206. https://doi.org/10.1016/j.apenergy.2017.01.047

Kim KY, Oh J, Han WS, Park KG, Shinn YJ, Park E (2018) Two-phase flow visualization under reservoir conditions for highly heterogeneous conglomerate rock: a core-scale study for geologic carbon storage. Sci Rep 8:1–10. https://doi.org/10.1038/s41598-018-23224-6

Klinkenberg LJ (1941) The permeability of porous media to liquids and gases. Paper presented at the API 11th Mid-year Meeting, Tulsa, Oklahoma

Ma T, Rutqvist J, Oldenburg CM, Liu W (2017) Coupled thermal-hydrological-mechanical modelling of CO2-enhanced coalbed methane recovery. Int J Coal Geol 179:81–91. https://doi.org/10.1016/j.coal.2017.05.013

Metwally YM, Sondergeld CH (2011) Measuring low permeabilities of gas-sands and shales using a pressure transmission technique. Int J Rock Mech Min 48(7):1135–1144. https://doi.org/10.1016/j.ijrmms.2011.08.004

Moridis GJ, Pruess K (2014) User's Manual of the TOUGH + Core Code v1.5: a general-purpose simulator of non-isothermal flow and transport through porous and fractured media, report LBNL-1871E. Lawrence Berkeley National Laboratory, Berkeley

Nasir O, Nguyen TS, Barnichon JD, Alain M (2017) Simulation of the hydro-mechanical behaviour of bentonite seals for the containment of radioactive wastes. Can Geotech J 54(8):1055–1070. https://doi.org/10.1139/cgj-2016-0102

Pan L, Oldenbur CM, Freifeld BM, Jordan PD (2017) Modeling the Aliso Canyon underground gas storage well blowout and kill operations using the coupled well-reservoir simulator T2Well. J Pet Sci Eng 161:158–174. https://doi.org/10.1016/j.petrol.2017.11.066

Roadifer RD, Scheihing MMH (2011) Impacts of the porosity permeability transform throughout the reservoir modelling workflow. In: SPE annual technical conference and exhibition, Denver Colorado, SPE 146574. https://doi.org/10.2118/146574-MS

Sander R, Pan Z, Connell LD (2017) Laboratory measurement of low permeability unconventional gas reservoir rocks: a review of experimental methods. J Nat Gas Sci Eng 37:248–279. https://doi.org/10.1016/j.jngse.2016.11.041

Wang Y, Liu S, Elsworth D (2015) Laboratory investigations of gas flow behaviors in tight anthracite and evaluation of different pulse-decay methods on permeability estimation. Int J Coal Geol 149:118–128. https://doi.org/10.1016/j.coal.2015.07.009

Yang Z, Sang Q, Dong M, Zhang S, Li Y, Gong H (2015) A modified pressure-pulse decay method for determining permeabilities of tight reservoir cores. J Nat Gas Sci Eng 27:236–246. https://doi.org/10.1016/j.jngse.2015.08.058

Zhang H, Liu J, Elsworth D (2008) How sorption-induced matrix deformation affects gas flow in coal seams: a new FE model. Int J Rock Mech Min Sci 45(8):1226–1236. https://doi.org/10.1016/j.ijrmms.2007.11.007

Zhao Y, Zhang L, Wang W, Tang J, Lin H, Wan W (2017) Transient pulse test and morphological analysis of single rock fractures. Int J Rock Mech Min Sci 91:139–154. https://doi.org/10.1016/j.ijrmms.2016.11.016

Zheng L, Rutqvist J, Xu H, Birkholzer JT (2017) Coupled THMC models for bentonite in an argillite repository for nuclear waste: illitization and its effect on swelling stress under high temperature. Eng Geol 230:118–129. https://doi.org/10.1016/j.enggeo.2017.10.002